CAMBRIDGE UNIVERSITY PRESS

A compact dual-band dual-linearly polarized waveguide slot array antenna with groove at waveguide bottom

Jun Gao [iD], Tianpeng Li, Hai Wang [iD], Xue Lei and Kexin Wang [iD]

Information Engineering University, Zhengzhou, China

Abstract

A dual-band dual-linearly polarized waveguide slot array antenna is proposed in this paper. Two orthogonal slots share a short-circuit wall on broad side. The horizontal and vertical slots, which actualize dual-frequency bands and dual-linear polarization, generate vertically polarized electric fields in 9.39–9.78 GHz and horizontally polarized electric fields in 11.62–12.3 GHz, respectively. The equivalent permittivity of the waveguide is changed by two grooves at the bottom of the waveguide, which improves phase velocity. Two grooves can also reduce the distance between the elements while suppressing the side lobes. Compared to filling the medium in the waveguide, two grooves have less losses. Moreover, the antenna is simple with one input port. The array antenna also overcomes the problems of beam scanning compared with the traditional waveguide slot array antenna. A 1×8 antenna array is fabricated and measured to verify the design. The horizontal polarization is formed in 9.39–9.78 GHz, the vertical polarization is generated in 11.62–12.3 GHz, and the antenna gain can reach 15 dBi.

Introduction

In modern wireless communication, waveguide-slotted arrays are good candidates for on-board and airborne antenna systems, especially dual-polarized antennas have been widely used [1–3].

In [3–6], a dual-polarized microstrip array antenna is designed; however, the microstrip antenna has more losses. In [7], a new material is used to reduce the losses, but it still reaches 0.17 dB. In [8–11], substrate-integrated waveguide dual-linear polarization antenna is designed. A 45° linearly polarized slot array antenna with differential dual-end feeding network is proposed in [9]. A novel dual-band dual-polarized aperture-shared slotted waveguide antenna array with high efficiency is presented in [11]. In [12–15], dual polarization is achieved by orthogonal slots on two waveguides, respectively. In [16], a dual-band antenna was designed using a gap waveguide as the transmission structure. In [17], dual polarization is achieved at the horizontal and vertical slots of the ridge waveguide and E-plane waveguide, respectively. In summary, all of them have complex transmission structure.

A dual-band dual-linearly polarized waveguide slot array antenna is proposed in this paper. Horizontal and vertical electric fields radiate from orthogonal slots on the broad side. Two grooves change the phase velocity and have less losses. A 1×8 array has been designed, which the pattern has no gate lobe and the side lobe level has not deteriorated. The measured results show horizontal and vertical polarization are realized in 9.39–9.78 and 11.62–12.3 GHz, respectively. The overall model is shown in Fig. 1, which includes radiation slots, groove, and power divider.

Antenna design

Lower and upper band design

Horizontal polarization is realized by a horizontal slot, which is shown in Fig. 2(a). The length of horizontal radiation slot is l_1. The vertical polarization is radiated from longitudinal slot with length l_2, as shown in Fig. 2(b). d_1 and d_2 are the distance between the slot's center and the short-circuit wall. The end of the waveguide is a short-circuit wall, and there is only one radiation slot on the broad side.

When electromagnetic waves transmit in WR-75, according to the waveguide wavelength formula:

$$\lambda_g = \frac{\lambda}{\sqrt{1 - (\lambda/2a)^2}}$$

$\lambda_g > \lambda$, where λ_g is the waveguide wavelength and λ is the free-space wavelength, a is broad dimension of waveguide. The distance between the center of the slot and the short-circuit wall is $\lambda_g/2$, which is about one-half of the waveguide wavelength.
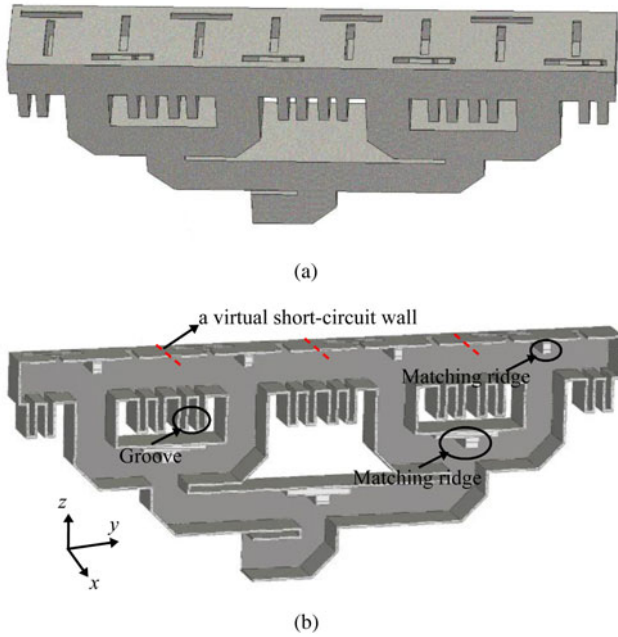
Fig. 1. Model of the antenna: (a) overview of the antenna and (b) sectional view of the antenna.

When simplifying array distribution as uniform linear array, the normalized shunt admittance of each slot is identically assumed as y, which is shown in Fig. 3. According to the transmission
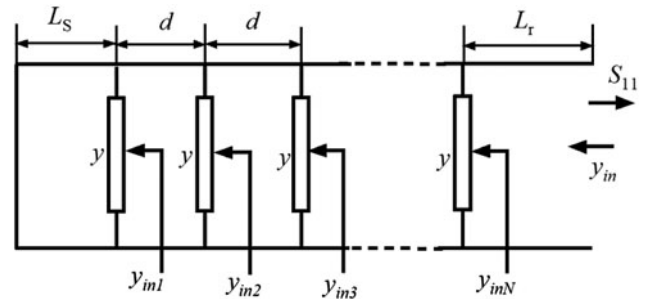

Fig. 2. (a) Model of horizontal polarization antenna; (b) the model of vertical polarization antenna; and (c) the simulated S_{11} ($l_1 = 12$ mm, $l_2 = 15$ mm).

Fig. 3. Equivalent transmission line model of N-element slotted uniform linear array terminated in a short circuit.
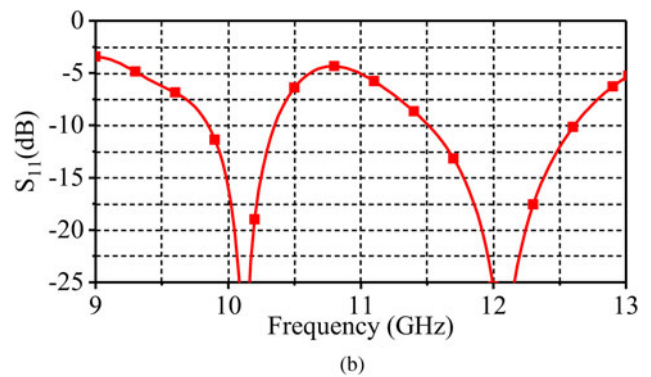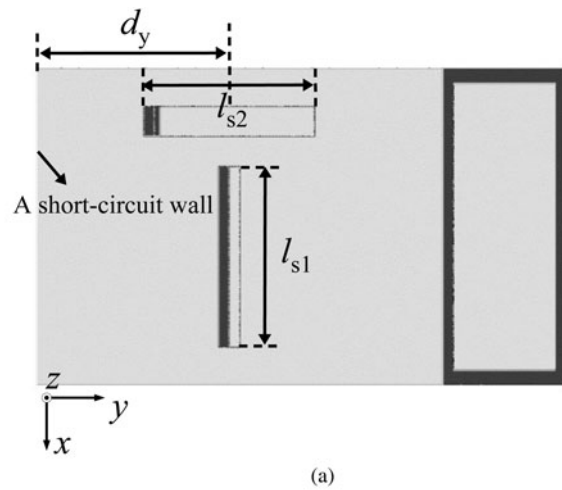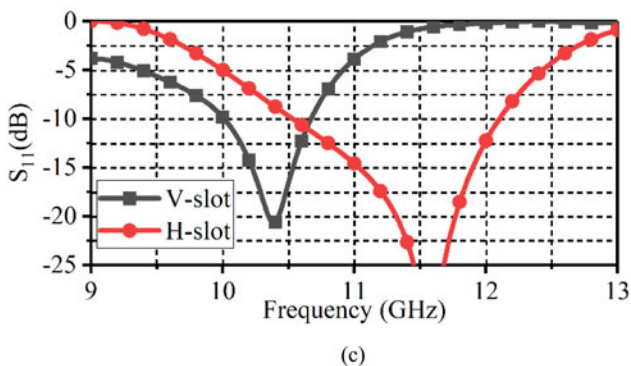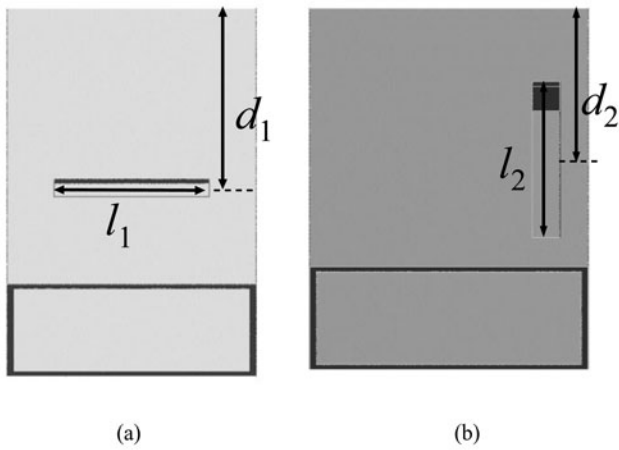

Fig. 4. Simulated dual-band unit of S_{11}.

line theory, we can define a function $f(y)$ as follows:

$$f(y) = y_{in}(y) - \frac{1 - S_{11}}{1 + S_{11}} = \frac{y_{inN} + jtg(\beta Lr)}{1 + y_{inN}tg(\beta Lr)} - \frac{1 - S_{11}}{1 + S_{11}} \quad (1)$$

Finding the complex roots of the $f(y) = 0$ can solve out y. The reflection coefficient S_{11} can be extracted from electromagnetic simulation software [18].

Fig. 2(c) depicts the simulated input impedance bandwidth (IBW) of the units. The IBW of the horizontal polarization unit for $S_{11} < -10$ dB is from 10–10.75 GHz. It is 10.6–12.1 GHz for $S_{11} < -10$ dB of the vertical polarization unit.
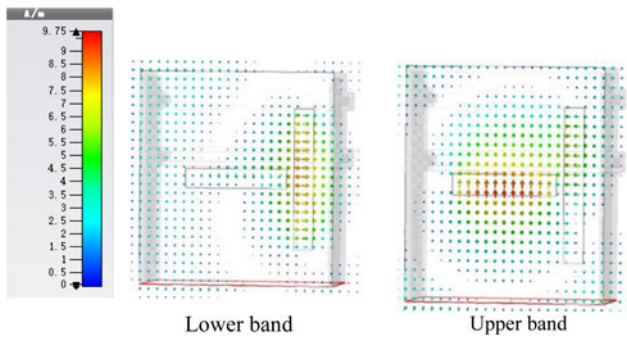
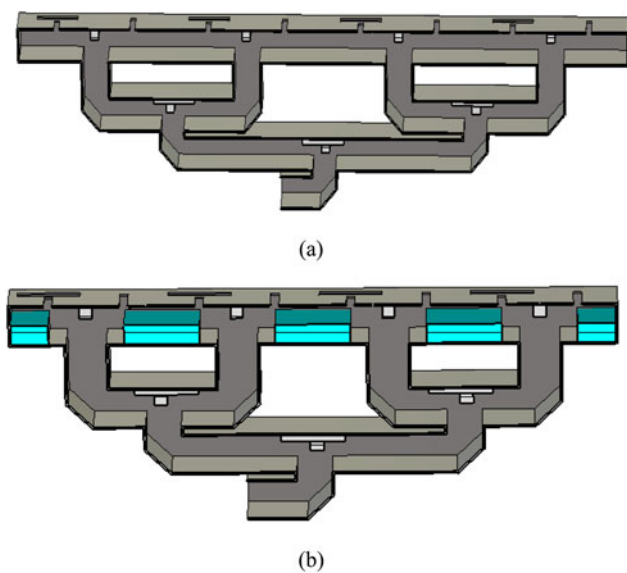Fig. 5. Simulated surface current distribution of the unit.

Fig. 6. (a) Without groove antenna array and (b) dielectric-added and non-grooved antenna array.

Dual-band unit design

The antenna must be able to generate vertically polarized electric fields and horizontally polarized electric fields to realize dual polarization. Figure 4(a) shows the structure. The broad side is slit orthogonal slots. The length of the two slots is l_{s1} and l_{s2}, respectively. Because the center position of the two slots is the same in the y direction, their distances from the short-circuit wall are d_y.

However, due to mutual coupling between the horizontal and vertical slots, which impacts the radiation, the resonant frequency has been shifted. The IBW is shown in Fig. 4(b). The $S_{11} < -10$ dB in 9.85–10.4 and 11.5–12.6 GHz. Figure 5 shows simulated current density at 10.25 and 12 GHz. A vertically polarized electric field is formed when the antenna operates at 10.25 GHz, and a horizontally polarized electric field is generated at 12 GHz. When the distance between two units is more than one free-space wavelength, the side lobe level will worse than −13 dB. The distance, along the y axis, between the center of the radiation slot and the radiation short-circuit wall is d_y. When the array is designed, the distance will have a significant impact on the side lobe.

Phase-compensated groove design

By adjusting the phase velocity, the side lobes can be suppressed and the antenna's compactness can be improved. Generally, adding the medium into the waveguide changes the phase velocity. However, there are two grooves with the same shape at the bottom of the waveguide in this paper. The dielectric-added and non-grooved antennas are shown in Fig. 6. The experiment is shown in Fig. 7, which is a radiation pattern comparison diagram of filling medium, with groove and without groove at 9.6 GHz. The operating frequency band is the same, but the side lobes of the antenna are different. The loss of the metal structure is less than filling medium. It can be found from Fig. 7 that the pattern side lobes for filling the medium and adding grooves are below −14.8 dB. The side lobe of the antenna pattern without adding the grooves is −11.9 dB. Adding grooves not only has less losses, but it can also effectively change the phase velocity. Because the waveguide is partially filled with medium, the equivalent dielectric constant is different from that of the medium itself. In addition, the equivalent dielectric constant generated by the groove is
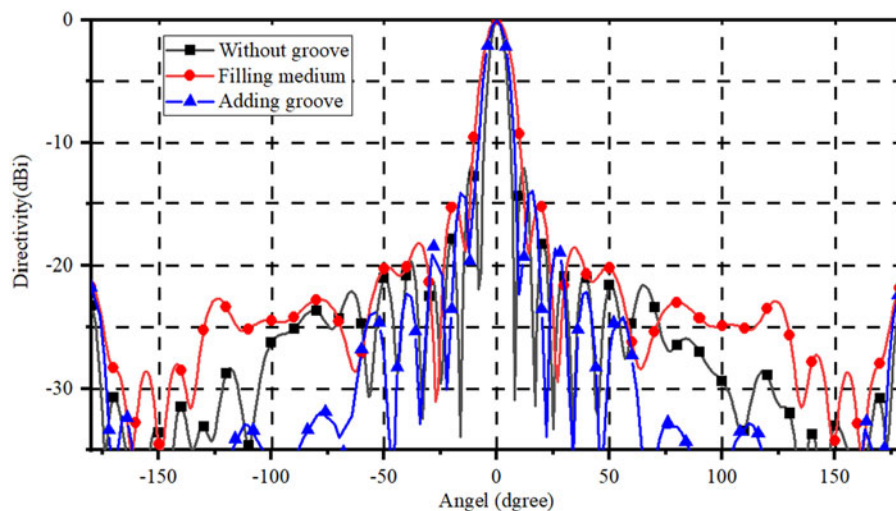

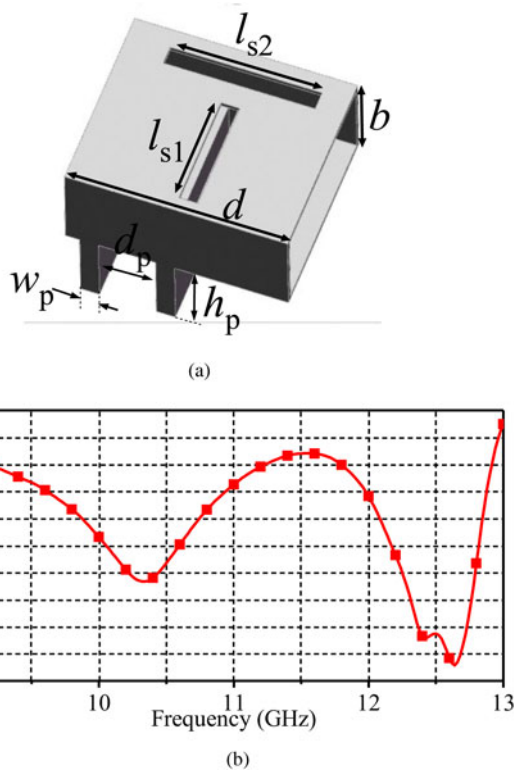Fig. 7. Patterns of three antenna array.

Fig. 8. (a) Model with two grooves at the bottom and (b) the S_{11} of the model.
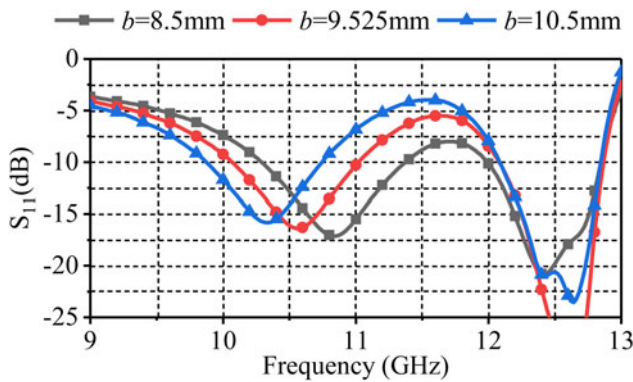

Fig. 9. Parametric analysis of the b of S_{11}.

Fig. 10. Parametric analysis of the d_p of $S_{11.}$
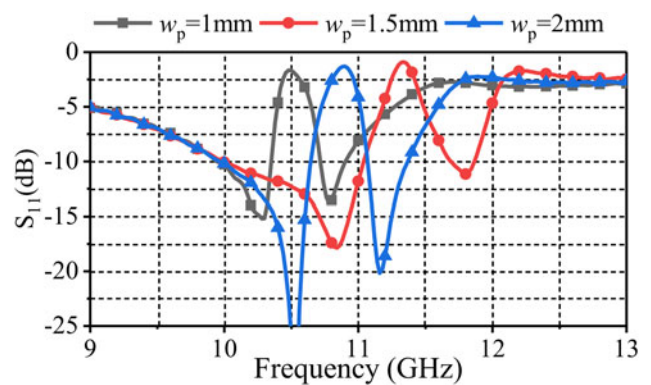
Fig. 11. Parametric analysis of the w_p of $S_{11.}$
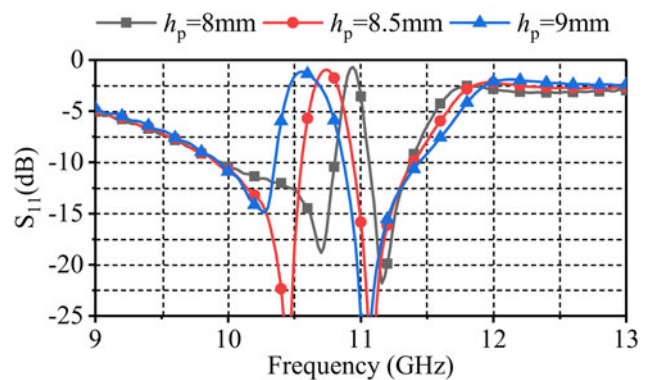
Fig. 12. Parametric analysis of the h_p of $S_{11.}$

dispersive, and different frequencies need to use different dielectric constants for alternative simulation. The configured dielectric constant of the filled medium set in the simulation varies with the frequency between 8.45 and 5.3.

When the antenna is arrayed, the distance between the units is d. The radiation slot and the short-circuit wall is $d/2$, two similar grooves are added, which effectively suppress the side lobes. The structure is shown in Fig. 8, the antenna becomes more compact.

Groove parameters analysis

A dual-polarized antenna was designed in the previous section. When the reflected electric field reaches radiation slots and comes in contact with the transmission electric field, the two electric fields with the same phase are superimposed on each other, which improves the radiation efficiency.

The narrow dimension b of the waveguide does not affect the λ_g of TE$_{10}$ mode. However, when the variation of b is combined with the groove design, the radiation of the horizontal slot will be major affected. When $b = 8.5$, $b = 9.5$ and b=10.5, the resonance frequency has been changed in the lower band, while the depth of resonance has been affected in the upper band. $b = 9.525$ mm is finally chosen to operate in better and more acceptable isolation (Fig. 9).

Table 1. Optimized parameters of the array antenna

Parameter	l_{s1}	l_{s2}	d_y	w_p	h_p
Values (mm)	12	15	9	1.5	8
Parameter	d	d_p	b		
Values (mm)	18	4.5	9.525		
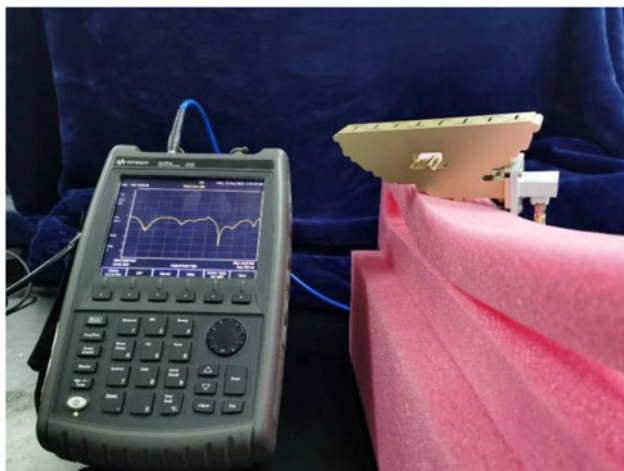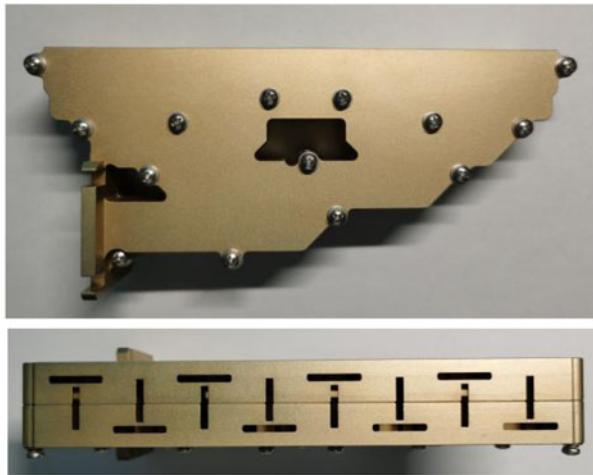
Fig. 13. Fabricated antenna.
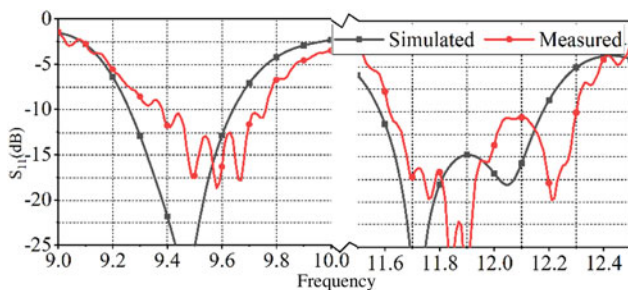
Fig. 14. Simulated and measured S_{11}.

Fig. 15. Measured and simulated normalized radiation patterns of VP array and HP array: (a) yoz-plane at 9.6 GHz, (b) xoz-plane at 9.6 GHz, (c) xoz-plane at 12 GHz, and (d) yoz-plane at 12 GHz.

As the groove affects the phase velocity, the values of w_p, h_p, and d_p are simulated in Figs 10–12, respectively. When $h_p = 8$ mm or $h_p = 9$ mm, the operating frequency is shifted and the performance becomes worse in the lower band. When $h_p = 8.5$ mm, the

$S_{11} < -10$ dB can be achieved in 9.95–10.55 and 10.95–11.45 GHz. When $w_p = 1$ mm or $w_p = 2$ mm, the operating frequency will shift, which has effect on the upper band seriously. When

Table 2. Comparison with some previous works

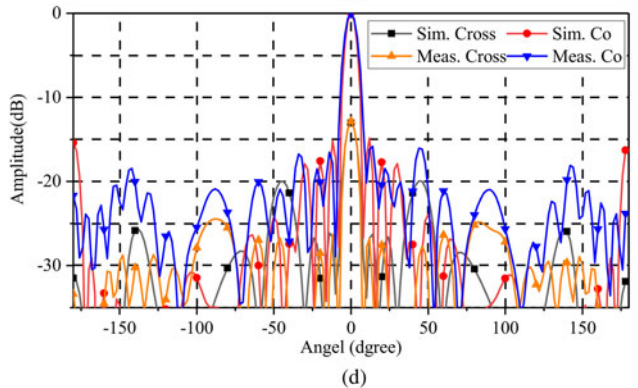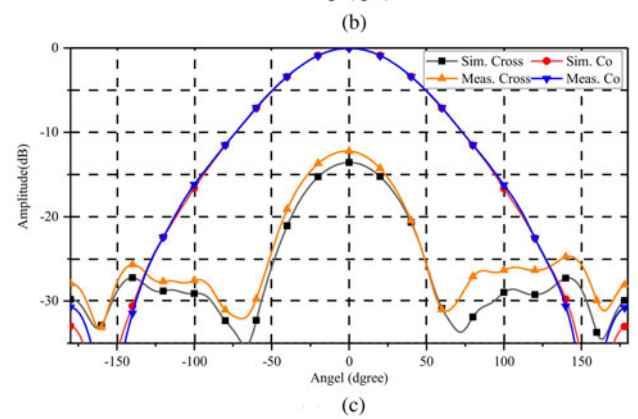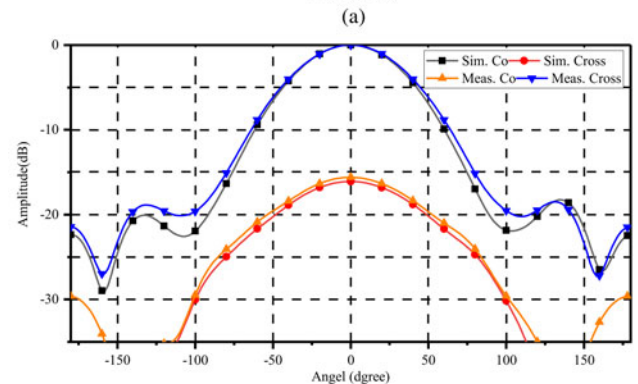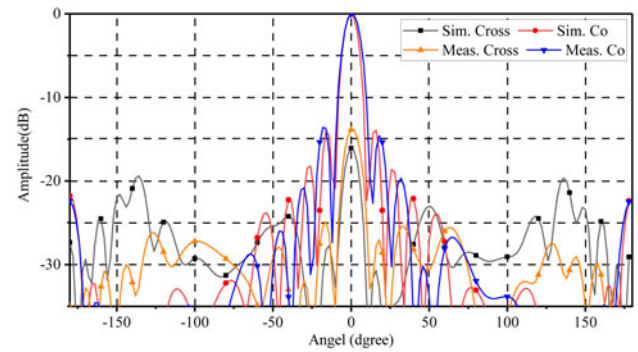| Ref.	Array	Type	Dielectric loss	Beam scanning	Port number
[4]	1 × 1	Microstrip	Yes	–	2
[5]	1 × 4	Microstrip	Yes	Yes	2
[6]	1 × 1	SIW	Yes	–	1
[7]	1 × 1	Waveguide	Yes	–	1
[8]	1 × 4	SIW	Yes	Yes	1
[14]	1 × 24	Waveguide	No	Yes	2
[15]	4 × 4	Waveguide	No	No	2
[19]	8 × 8	Microstrip	Yes	No	2
[20]	2 × 2	Waveguide	No	No	2
This work	1 × 8	Waveguide	No	No	1

$w_p = 1.5$ mm, the $S_{11} < -10$ dB can be achieved in 9.95–10.55 and 10.95–11.45 GHz. When $d_p = 5$ mm, the curve shifts to high frequency in the lower band; when $d_p = 7$ mm, the curve shifts to low frequency in the lower band, so d_p affects the lower band.

The length of the radiation slot l_{s1} and l_{s2} determines by the operating frequency and λ_g. The length l_{s1} and l_{s2} are adjusted for the case of with or without groove respectively. The simulation results are shown in Figs 4 and 8. When the values of l_{s1} and l_{s2} are inappropriate, the short-circuit wall cannot form the short-circuit requirements, so the energy of the antenna cannot be radiated normally.

Antenna array design and measurement

A 1 × 8 array antenna has been designed. Four 1 × 2 antenna arrays are connected by power divider. In order to simplify the design, when connecting 1 × 2 array elements, the short-circuit wall structure is removed in the connected position, and the electric field forms a virtual short-circuit wall in the same position. The overall structure is shown in Fig. 1, in which the dotted line part is a virtual short-circuit wall, and three virtual short-circuit walls are formed. Due to the coupling effect and edge effect of the array, the structural parameters in the array have been comprehensively optimized, and the final parameters are shown in Table I.

The prototype of the antenna is shown in Fig. 13, and the antenna dimension is 149 mm × 24.1 mm × 58.6 mm. The antenna can be functionally divided into two parts: power-divider feed and radiation structure. However, during manufacturing, in order to reduce the cutting of the current in the waveguide cavity, the antenna is divided into two symmetrical parts along the *y*-axis and connected by multiple screws.

According to the measured results, the S_{11} are shown in Fig. 14. From the results, $S_{11} < -10$ dB in 9.39–9.78 and 11.62–12.3 GHz, respectively. As the units of the array interact with each other, the operating frequency changes compared with the single unit. If considering the potential impact of measurement environment and fabrication tolerance , especially the influence of chamfer during machining, the measured results are basically consistent with the simulation results. The antenna can achieve $S_{11} < -10$ dB in lower and upper bands, respectively.

The pattern is one of the important indicators, which is shown in Fig. 15. The antenna patterns of vertical polarized (VP) and horizontal polarized (HP) on the *xoz* and *yoz* planes were measured

at 9.6 and 12 GHz, respectively. As can be seen from Fig. 15, the side lobe level can reach −14 dB and no grating lobe is generated in the pattern, which proves the groove can effectively compensate the phase difference between the units. The cross-polarization level is about −14 dB. The antenna structure is simple, and the beam is not scanned. Similar antennas mentioned in the paper are compared in Table 2.

Conclusion

In this paper, we designed a dual-linear dual-band waveguide slot antenna with low side lobe. Two grooves are added at the bottom of the antenna. Orthogonal slots slit on the broad side realizes dual polarization. Dual band is realized in 9.39–9.78 GHz and 11.62–12.3 GHz. The former is horizontal polarization, and the latter is vertical polarization. The side lobe level of the antenna can reach −14 dB.

Conflict of interest. The authors report no conflict of interest.

References

1. **Wang W, Jin J, Liang X-L and Zhang Z-H** (2006) Broadband dual polarized waveguide slotted antenna array, *2006 IEEE Antennas and Propagation Society International Symposium*, pp. 2237–2240.
2. **Tang Z, Liu J, Lian R, Li Y and Yin Y** (2019) Wideband differentially fed dual-polarized planar antenna and its array with high common-mode suppression. *IEEE Transactions on Antennas and Propagation* **67**, 131–139.
3. **Li H, Kang L, Wei F, Cai Y and Yin Y** (2017) A low-profile dual-polarized microstrip antenna array for dual-mode OAM applications. *IEEE Antennas and Wireless Propagation Letters* **16**, 3022–3025.
4. **Kasemodel JA and Volakis JL** (2010) A planar dual linear-polarized antenna with integrated balun. *IEEE Antennas and Wireless Propagation Letters* **9**, 787–790.
5. **Lian R, Wang Z, Yin Y, Wu J and Song X** (2016) Design of a low-profile dual-polarized stepped slot antenna array for base station. *IEEE Antennas and Wireless Propagation Letters* **15**, 362–365.
6. **Kahar M and Mandal MK** (2019) Dual-band dual-polarized SIW filtering antenna. *2019 IEEE International Symposium on Antennas and Propagation and USNC-URSI Radio Science Meeting*, pp. 331–332.
7. **He Y, Ding N, Zhang L, Zhang W and Du B** (2015) Short-length and high-aperture-efficiency horn antenna using low-loss bulk anisotropic

metamaterial. *IEEE Antennas and Wireless Propagation Letters* **14**, 1642–1645.

8. **Zhao X-Y, Ban Y-L, Sun Q and Li X-F** (2019) Dual-polarization beam scanning antenna array based on TE01/TE10 Modes. *2019 International Symposium on Antennas and Propagation (ISAP)*, pp. 1–2.

9. **Zhou H and Hong W** (2015) 45° Polarized slot array antenna with differential dual-end feeding network for vehicle applications. *2015 International Symposium on Antennas and Propagation (ISAP)*, pp. 1–3.

10. **Sanchez-Olivares P, Masa-Campos JL, Kumar P and Garcia-Marin E** (2019) Dual polarized travelling-wave array antenna formed by printed cross slots. *2019 13th European Conference on Antennas and Propagation (EuCAP)*, pp. 1–5.

11. **Ding YR and Cheng YJ** (2019) Ku/Ka dual-band dual-polarized shared-aperture beam-scanning antenna array with high isolation. *IEEE Transactions on Antennas and Propagation* **67**, 2413–2422.

12. **Chen M, Fang X-C, Wang W, Zhang H-T and Huang G-L** (2020) Dual-band dual-polarized waveguide slot antenna for SAR applications. *IEEE Antennas and Wireless Propagation Letters* **19**, 1719–1723.

13. **Li T, Meng H and Dou W** (2014) Design and implementation of dual-frequency dual-polarization slotted waveguide antenna array for Ka-band application. *IEEE Antennas and Wireless Propagation Letters* **13**, 1317–1320.

14. **Sanchez-Olivares P, Masa-Campos JL, Garcia-Marin E, Barrio-Tejedor D and Kumar P** (2020) Dual-linearly polarized travelling-wave array antenna based on triple plus slots fed by square waveguide. *AEU-International Journal of Electronics and Communications* **119**, 153176.

15. **Ferrando-Rocher M, Herranz-Herruzo JI, Valero-Nogueira A and Baquero-Escudero M** (2021) Dual-band single-layer slot array antenna fed by K/Ka-band dual-mode resonators in gap waveguide technology. *IEEE Antennas and Wireless Propagation Letters* **20**, 416–420.

16. **Zhang H-T, Wang W, Chen M, Zou Y-Q and Liang X-L** (2019) A dual band dual-polarization aperture-shared slotted waveguide antenna array with high efficiency, 2019 8th Asia-Pacific Conference on Antennas and Propagation (APCAP), pp. 44–45.

17. **Wang W, Jin J, Lu J-G and Zhong S-S** (2005) Waveguide slotted antenna array with broadband, dual-polarization and low cross-polarization for X-band SAR applications. *IEEE International Radar Conference* **2005**, 653–656.

18. **Wang W, Zhong S-S, Zhang Y-M and Liang X-L** (2006) A broadband slotted ridge waveguide antenna array. *IEEE Transactions on Antennas and Propagation* **54**, 2416–2420.

19. **Yashodha BH, Sujatha BK, Vishwakarma NK and Srijeeth CA** (2020) Ku band dual linear polarized antenna for satellite communication. *2020 IEEE 7th Uttar Pradesh Section International Conference on Electrical, Electronics and Computer Engineering (UPCON)*, pp. 1–4.

20. **Pang Z-Y, Ma X-Y, Zhuo X-Q, Wang C-Y, You S-S and Huang G-L** (2021) A dual-linear polarized wideband waveguide-based antenna block. *2021 International Conference on Microwave and Millimeter Wave Technology (ICMMT)*, pp. 1–3.

Jun Gao obtained his MS degree in electronic science and technology from the University of Information Engineering in 2018. His main research interests include aperture antennas and beam-steering antennas.

Tianpeng Li received his BS and MS degrees from Air Force Engineering University, Xi'an, China, in 2012 and 2016, respectively. He is currently working at the Information Engineering University. His main research interests include antennas and propagation.

Hai Wang received his BS degree from Logistical Engineering University, Chongqing, China, in 2015. He is currently pursuing his MS degree at Information Engineering University. His main research interests include aperture antennas, wideband antennas, and wide axial ratio antennas.

Xue Lei received her BS and MS degrees from Information Engineering University in 1989 and 2000, respectively. She is currently working at Information Engineering University. Her main research interests include antennas and electromagnetic wave propagation.

Kexin Wang obtained his MS degree in electronic science and technology from the University of Information Engineering in 2022, and he is currently pursuing his Ph.D. in information and communication engineering. His current research interests include phased arrays, side lobe suppression, and optimization algorithms.